Spectroscopy, microscopy and theoretical study of NO adsorption on MoS$_2$ and Co–Mo–S hydrotreating catalysts

Nan-Yu Topsøe [a,*], Anders Tuxen [b], Berit Hinnemann [a,*], Jeppe V. Lauritsen [b,*], Kim G. Knudsen [a], Flemming Besenbacher [b], Henrik Topsøe [a]

[a] Haldor Topsøe A/S, Nymøllevej 55, DK-2800 Kgs. Lyngby, Denmark
[b] Interdisciplinary Nanoscience Center (iNANO), and Department of Physics and Astronomy, Aarhus University, DK-8000 Aarhus C, Denmark

ARTICLE INFO

ABSTRACT

Infrared (IR) spectroscopy using NO as a probe molecule has been one of the important methods for characterizing hydrotreating catalysts, since this technique provides information on the nature and quantity of active edge sites of these catalysts. However, due to the strong adsorption of NO, which may lead to significant edge reconstructions, it has not been clear, how the characteristics of the adsorption complexes may reflect the nature of the original edge sites. By combining IR spectroscopy measurements with scanning tunneling microscopy (STM) experiments and density functional theory (DFT) calculations, we present new atomic-scale insight into the nature of NO adsorption on MoS$_2$ and Co–Mo–S nanoclusters. The DFT calculations and STM experiments show that NO does not adsorb at fully sulfided MoS$_2$ edges not containing hydrogen. However, typical sulfided catalysts will have hydrogen present at the edge in the form of S–H groups. For such samples, the results indicate a "push–pull" type mechanism involving simultaneous vacancy creation, NO adsorption and H$_2$S release. This mechanism is observed to dominate in the IR experiments. In STM experiments, stable vacancies can be generated by dosing atomic hydrogen, and these vacancies are observed to adsorb NO dimers. The detailed nature of the adsorption is revealed by DFT. IR measurements recorded during temperature-programmed desorption (TPD) show the presence of several NO adsorption complexes and the assignment to specific species is achieved by comparison to calculated frequencies and adsorption energies obtained from DFT. The results show that mononitrosyl species dominate at the Mo-edges, whereas stable dinitrosyl species are found at both the unpromoted and the Co-promoted S-edges. Thus, based on the present results, it is possible to use NO as a probe molecule to obtain detailed atomic-scale information on hydrotreating catalysts and the origins of activity differences.

© 2011 Published by Elsevier Inc.

1. Introduction

In order to meet the increasing demands for the production of ultra clean transportation fuels [1], there is a need to obtain an atomic-scale understanding of the nature of the active sites involved in different hydrotreating reactions for both unpromoted and promoted MoS$_2$-based catalysts [2–8]. Specifically, a better insight into the sites involved in hydrogenation and hydrogenolysis reactions in both unpromoted and promoted MoS$_2$-based catalysts is desirable, since the relative significances of the two types of reactions depend strongly on both the feedstocks and the required conversions [2,9–13]. For many years, information regarding the surface binding sites in hydrotreating catalysts has mainly been obtained by the use of different spectroscopic techniques [2], and

one of the most important approaches has been to follow the adsorption of different probe molecules such as NO [14–32] and CO [28,33–42] by means of infrared (IR) spectroscopy. For example, IR studies of NO adsorption made it possible to distinguish different adsorption complexes for both unpromoted and promoted catalysts [16–18,43]. This is a distinct advantage compared to other extensively used characterization methods like oxygen chemisorption [44]. Combined IR_NO studies and extended X-ray adsorption fine structure (EXAFS) spectroscopy experiments on sulfided Mo/Al$_2$O$_3$ catalysts showed that NO molecules were adsorbed on MoS$_2$ edges and not on the basal planes [45]. Typical IR spectra of Co/Al$_2$O$_3$, Mo/Al$_2$O$_3$ and Co–Mo/Al$_2$O$_3$ catalysts after sulfidation are shown in Fig. 1 (adapted from Ref. [43]). These spectra show that it is possible to distinguish between NO adsorption on the Co and Mo sites, since some of the bands do not overlap. In Fig. 1b, we show for a series of catalysts with constant Mo loading a plot of the NO-IR absorbance of the high-frequency band due to NO adsorbed on Co (around 1850 cm^{-1}) and the low-frequency
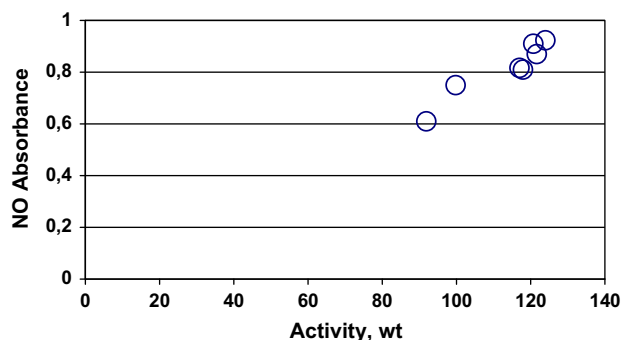
* Corresponding authors. Fax: +45 4593 2999 (B. Hinnemann).
E-mail addresses: nat@topsoe.dk (N.-Y. Topsøe), behi@topsoe.dk (B. Hinnemann), jvang@inano.au.dk (J.V. Lauritsen).
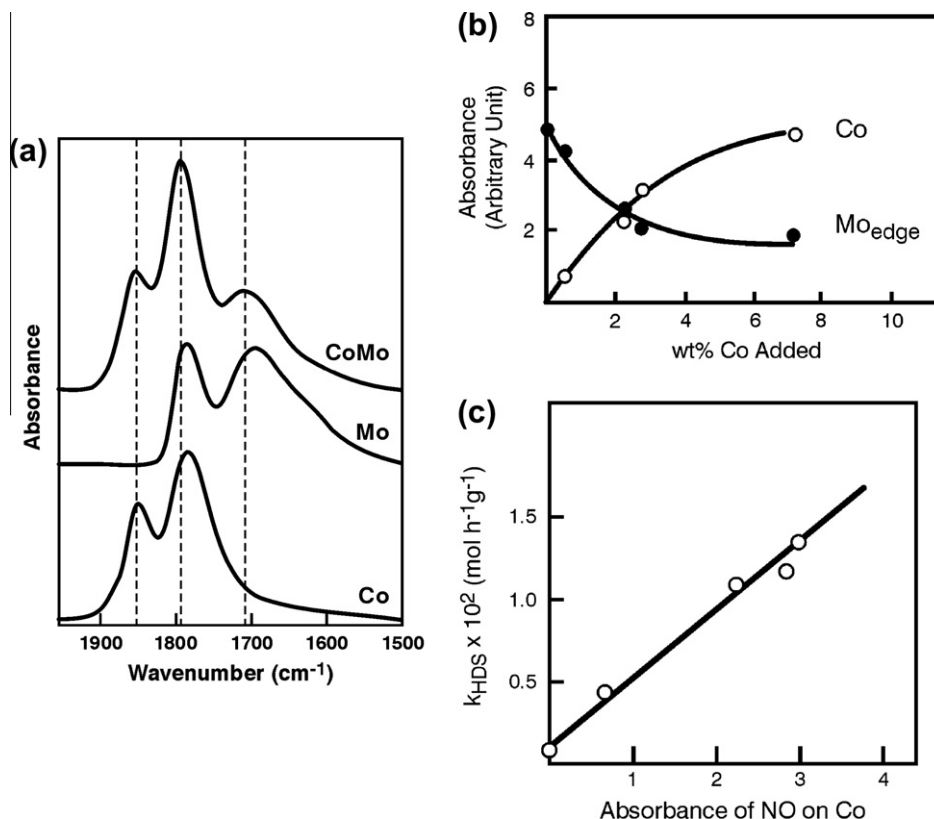
Fig. 1. (a) IR spectra of NO adsorbed on sulfided 2% Co/Al_2O_3, 8% Mo/Al_2O_3 and 2%Co 8%Mo/Al_2O_3. (b) Absorbance of IR bands of NO adsorbed on Co (1850 cm^{-1}) and Mo (1690 cm^{-1}) plotted as function of Co/Mo ratio at constant Mo loading. (c) Thiophene HDS activities vs. absorbance of IR band of NO adsorbed on Co. The figure is adapted from Ref. [43].

band due to NO adsorbed on Mo (around 1690 cm^{-1}) as function of Co loading. The simultaneous decrease in the absorbance of the Mo–NO band and increase in the Co–NO band revealed that the Co atoms are located at the MoS_2 edges, and this provided important new insight into the nature of the Co–Mo–S structure. Fig. 1c shows that there is a linear correlation between the absorbance of NO on the Co sites and the thiophene HDS catalytic activity. This correlation demonstrated clearly that NO probes the Co-promoted sites in Co–Mo–S, which are responsible for the activity increase. For the less-active unpromoted Mo/Al_2O_3 catalysts, IR results also showed correlations between the activity and the amount of MoS_2 edge sites titrated by NO [45]. NO adsorption is also a useful tool for characterizing industrial catalysts, and Fig. 2 shows data for NO absorbance on Co sites versus real feed catalytic activity for industrial-type hydrotreating catalysts. Even though the corre-

lation is less clear than for the model catalysts, this example nonetheless illustrates the usefulness of NO adsorption to assess catalytically active sites and explains the popularity of this method.

In view of the usefulness of this technique, there has for many years been a strong interest in obtaining a detailed understanding of the nature and location of the different adsorption complexes. In an early approach for obtaining such knowledge, the observed IR frequencies for hydrotreating catalysts were compared to those observed for well-defined NO-containing inorganic metal sulfur clusters [46]. Such studies showed that the adsorption complexes had many similarities to dinitrosyl complexes exhibiting pseudotetrahedral coordination around the adsorbing atom. Also isotopic exchange studies [47] were consistent with a dinitrosyl behavior of the adsorption complex. More recently, detailed desorption [24], electron paramagnetic resonance [48] and magnetic studies [31] have also provided further insight, but many questions still remain. For example, in view of the strong bond of the edge sites with NO, it is possible that the local geometry of the adsorption complex differs from that of the original surface sites, such that significant reconstructions on the edges of the MoS_2 nanoclusters may take place [16–18]. In order to avoid substantial surface reconstructions, it may be advantageous to use CO as a probe molecule [40]. However, the frequencies of the NO adsorption bands are more sensitive toward changes in the catalyst structure, and the NO adsorption technique has found widespread use in the study of many catalyst systems [16–18,29]. Both CO and NO adsorption on hydrotreating catalysts have recently been studied by density functional theory (DFT). CO adsorption has been studied theoretically on MoS_2, Co–Mo–S and Ni–Mo–S catalysts [40,41,49–53] and NO adsorption on unpromoted MoS_2 catalysts [54,55].

Fig. 2. Absorbance of IR band of NO adsorbed on Co site (1850 cm^{-1}) on sulfided $CoMo/Al_2O_3$ industrial catalysts versus real feed activity per weight.

In recent years, tunneling microscopy (STM) studies [56–62,63] have improved the fundamental understanding of the molecular aspects of sulfide catalysts. In particular, when such studies have been combined with DFT calculations [57,58,60–62,64–78] this has given unique atomic-scale insights into the structure and reactivity of both unpromoted MoS_2 and promoted Co–Mo–S and Ni–Mo–S nanostructures. In particular, the interplay of the STM and the DFT techniques has resulted in a more complete understanding than either of the techniques could provide alone [79]. STM and DFT have also allowed new insight into the adsorption of different molecules on hydrotreating catalysts and in a recent study [80]; we used these techniques to re-investigate earlier IR results and proposals [81,82] regarding the adsorption of pyridine on MoS_2 nanoclusters. The combination of IR, STM and DFT proved very useful, and in the present study we use this combined approach to obtain new insight into the adsorption of NO on MoS_2 and Co–Mo–S nanoclusters. In order to obtain more detailed IR information, the NO adsorption bands are also recorded during temperature-programmed desorption (TPD) [25]. These results are compared to energies and frequencies calculated by DFT and provide additional means for identifying the origin of the different IR bands.

An interesting conclusion of this study is that stable sulfur vacancies (or coordinatively unsaturated sites) existing prior to adsorption may not be a prerequisite for NO adsorption. Instead, we find that the formation of the adsorption complex can take place via a "push–pull" type mechanism involving a drastic rearrangement of the surface atoms. In this situation, S-edge atoms are removed and NO is adsorbed and H_2S is released in a concerted process. In previous theoretical studies, a push–pull mechanism was also considered by Wen et al. for NO adsorption [54,55] and also for CO adsorption [50]. By this push–pull process, one avoids the energetically unfavorable step of creating stable vacancies; and for the samples used in the IR experiments, the H_2S release appears to be linked to the presence of S–H groups prior to NO adsorption. In the STM experiments, it is possible to create stable vacancies by dosing with atomic hydrogen, and these vacancies may subsequently adsorb NO. Thus, in this case, a classical two-step process may take place. By calculating the energetics and vibrational frequencies, we can obtain useful information on the origin of differences in bands and thereby also get more insight into the origin of the activity correlations.

2. Experimental

2.1. IR experiments

The Mo/Al_2O_3 catalyst studied consists of 8 wt.% Mo and was prepared by depositing the active material onto an η-Al_2O_3 carrier (surface area, 230 m^2/g) via the incipient wetness method using ammonium heptamolybdate followed by drying and calcining in air at 500 °C for 2 h. The Co-promoted catalysts were prepared by co-impregnation followed by similar drying and calcination procedure.

For the IR studies of NO adsorption, the catalyst sample in the form of a self-supporting wafer with a thickness corresponding to 4.7 mg/cm^2 was sulfided in situ in the IR cell in a gas flow consisting of 2% H_2S in H_2 at 450 °C for 2 h. This was followed by a N_2 flush treatment at 400 °C for 14 h before cooling to room temperature. NO adsorption was carried out after an evacuation for 1 h to 10^{-6} mbar at room temperature. For NO desorption experiments, the sample was evacuated during heating and spectra were measured while the temperature was held constant at 50 °C intervals. The IR spectra were recorded on a Bio-Rad FTS 575C FTIR spectrometer equipped with a MCT detector.

2.2. STM experiments

The STM experiments were performed in an ultrahigh vacuum (UHV) chamber with a base pressure below 1×10^{-10} mbar. The UHV setup includes equipment for synthesis of MoS_2 nanoclusters and surface characterization tools, including a home-built variable temperature Aarhus STM [83], which is capable of achieving atomic resolution on MoS_2 nanoclusters on a routine basis. For the NO adsorption studies, we have used a well-characterized planar model system of the hydrotreating catalysts consisting of MoS_2 nanoclusters synthesized on an Au(1 1 1) substrate. We have previously used this system successfully to reveal the atomic-scale structure of MoS_2 and promoted Co–Mo–S nanoclusters [56–63]. The full details concerning the preparation and characterization of the HDS model system and the atomic-scale structure of the MoS_2 nanoclusters have been published previously (see e.g. Refs. [56,63]). Our previous studies [66,84] have also shown that the Au substrate is sufficiently weakly interacting with MoS_2 so that the edges are only weakly perturbed geometrically and electronically, which ensures that mainly adsorption configurations reflecting the interaction of NO with "free" MoS_2 is probed in the STM model studies. Gaseous nitric oxide (NO) was dosed to the UHV system from a lecture bottle (Praxair, nominal purity 2.0) through an all-metal leak valve. The gas purity was monitored prior to the experiment using a quadrupole mass spectrometer (QMS), and it revealed a pure NO gas with trace amounts of N_2, N_2O and O_2. To probe the interaction between NO and a sulfur vacancy in the STM experiment, the fully sulfided MoS_2 clusters were activated by treating with atomic (pre-dissociated) hydrogen, since this procedure allows us to mimic vacancy creation under UHV conditions. Molecular hydrogen does not react with the MoS_2 nanoclusters at UHV-compatible pressures less than 1×10^{-6} mbar, but as demonstrated in Refs. [56,61,85], a dose of atomic hydrogen (5–15 min) leads to formation of sulfur vacancies and S–H groups on the edges. The atomic hydrogen was produced by backfilling the chamber with 1×10^{-6} mbar of hydrogen while keeping a hot (~1800 °C) W filament in the proximity of the substrate at 180 °C. Subsequently, the hydrogen was pumped away, and the substrate was cooled to room temperature. NO was then dosed for 3 min by backfilling the UHV chamber to a total pressure of 7×10^{-8} mbar of NO. The subsequent STM images were all recorded close to room temperature.

2.3. DFT calculations

The theoretical calculations are based on density functional theory using an infinite stripe model of MoS_2, analogous to Refs. [57, 66, 77, 78, 80]. Fig. 3 depicts the used stripe, which exposes the $(10\bar{1}0)$ Mo-edge on one side and the $(\bar{1}010)$ S-edge on the other side. We use a stripe containing two Mo atoms in the x-direction and four Mo atoms in the y-direction (denoted 2 × 4 model). We have recalculated selected structures for a larger 2 × 6 model and find that the vibrational frequencies change less than 5 cm^{-1} and the binding energies less than 5 kJ/mol. For the simulations of STM images, we use a larger 4 × 4 model to be able to simulate the lower NO coverage seen in the STM experiments. The stripes are separated by 14.8 Å in the z-direction and 9 Å in the y-direction.

This model allows us to investigate numerous structures for NO adsorption, which is important, since the atomic structure and the sulfur and hydrogen coverages on the Mo-edge, S-edge and Co–Mo–S-edge depend on the surrounding gas atmosphere [60, 66, 68]. For sulfiding synthesis conditions, it is known from the STM and DFT studies that the MoS_2 clusters are triangular and only the Mo-edge covered with sulfur dimers is exposed [57]. Fig. 3 shows the most stable structure of the Mo-edge under these
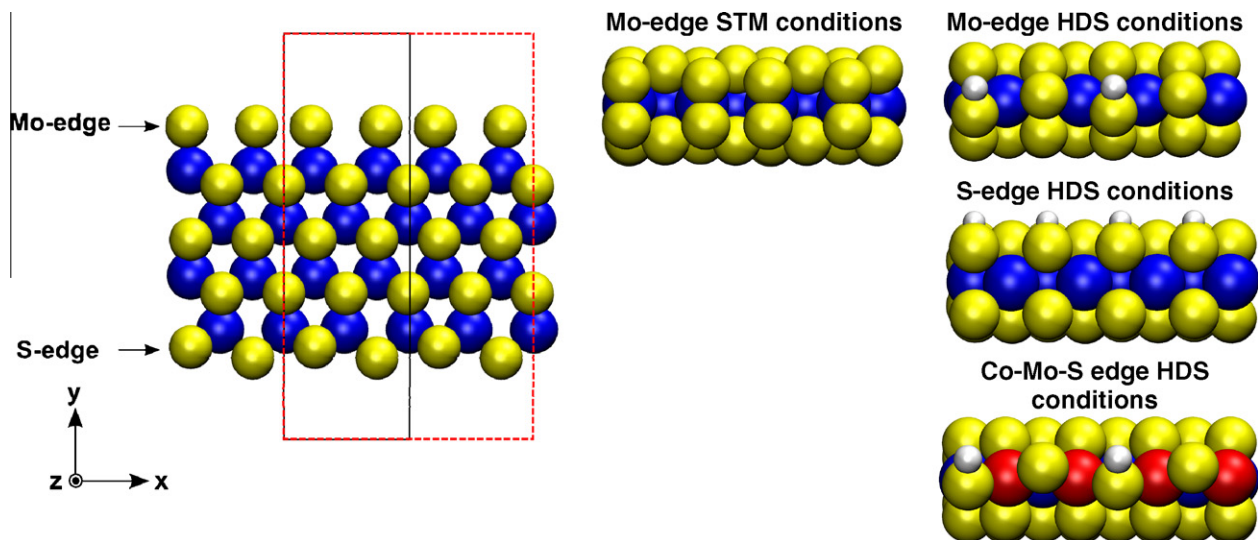
Fig. 3. To the left, the employed MoS$_2$ slab for all calculations. The 2 × 4 unit cell is indicated in solid black lines and the 4 × 4 unit cell used for the STM calculations is indicated in dashed red lines. To the right side, views of the most stable edge structures under STM and HDS conditions, which are taken as reference structures in the present studies. Color code for this and all subsequent figures: sulfur (yellow), molybdenum (blue), cobalt (red, large balls), nitrogen (light blue), oxygen (red, small balls), hydrogen (white). (For interpretation of the references to color in this figure legend, the reader is referred to the web version of this article.)

conditions. Under HDS conditions corresponding to P(H$_2$)/P(H$_2$S) ∼ 100, both the Mo-edge and the S-edge are exposed and clusters have a hexagonal or truncated triangular shape [60]. Under these conditions, the Mo-edge is terminated by sulfur monomers and hydrogen with a coverage of 0.25–0.5, whereas the sulfur edge is terminated by sulfur dimers and hydrogen on every dimer [74,77]. The promoted Co–Mo–S-edge under HDS conditions is terminated by sulfur monomers and a hydrogen coverage of 0.25 [78]. However, since we use a 2 × 4 unit cell where only an integer amount of hydrogen can be in the cell, we use the structure with a hydrogen coverage of 0.5 as the reference structure. We have tested that none of the conclusions are changed with respect to referencing to a structure with lower hydrogen coverage. The Mo-edge, S-edge and Co–Mo–S-edge reference structures for HDS conditions are shown in Fig. 3.

DACAPO, a plane-wave density functional theory code, is used in the calculations [86], [87]. In the 2 × 4 model, the Brillouin zone is sampled by a Monkhorst–Pack k-point set [88] with four k-points in the x-direction and with one k-point in the y- and z-directions (4 × 1 × 1 k-point set). For the larger 4 × 4 model, we use a 2 × 1 × 1 k-point set. We tested k-point sets with more k-points in the x-direction and found that total energies differ less than 0.01 eV. We use a 30 Rydberg plane-wave cutoff and 45 Rydberg density-wave cutoff [89]. Ultrasoft pseudopotentials [90] are used except sulfur, for which a soft pseudopotential is used [91]. The Fermi temperature is chosen to be $k_BT = 0.1$ eV, and all the energies are extrapolated to zero electronic temperature. For Co–Mo–S, all calculations are carried out spin-polarized due to the magnetic moment of the Co atoms [92]. As the revised Perdew–Burke–Ernzerhof (RPBE) exchange–correlation (XC) functional [86] is known to give improved binding energies compared to the PW91 [93] functional [74,86], we use it in this study. To assess the influence on XC functional on calculated vibrational frequencies, we recalculate structures and frequencies with the PW91 functional for the most important structures. This recalculation is done with the correct lattice parameter for PW91 and relaxation of the structure. We calculate an equilibrium lattice parameter of $a = 3.24$ Å for the RPBE functional and $a = 3.22$ Å for the PW91 functional, both in good agreement with the experimental lattice constant of 3.16 Å [94]. We relax all structures, until all

force components for all atoms are below 0.02 eV/Å. We also tested tighter force convergence criteria, but found negligible differences in structures and energies.

The calculations of the vibrational frequencies are performed using numerical derivatives obtained by three-point finite differences with 0.02 Å displacements in all three directions. We also tested a displacement of 0.01 Å and found that the resulting vibrational frequencies only differ by few wavenumbers. We only allow the N and O atom in the NO molecule to vibrate and keep the other atoms fixed. As DFT is not perfect in calculating the vibrational frequency for the NO molecule, we need to scale the calculated vibrational frequencies with a constant factor to be able to compare the calculated frequencies to the ones observed by IR spectroscopy. We calculate the vibrational frequency for the NO molecule in the gas phase to be 1949 cm^{-1} with the RPBE functional and 1948 cm^{-1} with the PW91 functional, both calculations are with 0.02 Å displacement. For comparison, a 0.01 Å displacement gives 1953 cm^{-1} for RPBE and 1948 cm^{-1} for PW91. The experimental NO frequency is 1876 cm^{-1} [95]. It is noted that this frequency contains a considerable anharmonicity term and the experimental frequency with removed anharmonicity is 1904 cm^{-1} [95]. To judge the accuracy of the DFT calculations, the calculated frequencies should be compared to the value 1904 cm^{-1}, and here we find that the agreement is fair and in line with usual DFT accuracy. However, for scaling the frequencies, we choose to scale the frequencies to the observed frequency 1876 cm^{-1} so that the direct comparison of theory and experiment is possible. Thus, the scaling factor is 0.96 for both RPBE and PW91 and is applied to all calculated frequencies. Comparing the vibrational frequencies calculated with the RPBE and PW91 exchange–correlation functionals, it is noted that for most structures the scaled frequencies are quite close to each other, differing by only 10–20 cm^{-1}. This gives an estimate of the influence of the exchange–correlation functional on the calculated vibrational frequencies. In the paper, we mainly discuss the RPBE values but note that all conclusions drawn in this paper are equally valid for the PW91 values. By using the same scaling factor for all calculations, we assume the extent of anharmonicity for free and adsorbed NO to be the same. This is certainly an approximation in line with the other outlined approximations, and as a result, the accuracy of the calculated frequencies is on

the order of 20 cm^{-1}. For the present conclusions, this is sufficient, and a detailed DFT study of anharmonicity is therefore outside the scope of the present study. Along the same lines, we only consider the vibrational frequencies and do not calculate absolute intensities, as the methodology for such calculations still is being developed.

Simulated STM images are calculated within the Tersoff–Hamann formalism, in which the STM images are represented as contours of local density of states at the Fermi level projected to the tip apex position. We used the same parameters as in earlier publications [66,80], since they were adjusted such that the calculated corrugation on the basal plane of the MoS$_2$ nanocluster matches the experimentally observed one. We tried both an s-type and p-type tip, but report only the s-type results here since the p-type tip did not change the general trends of the images. We used a contour value $\rho(r_0, \varepsilon_F) = 8.3 \times 10^{-6}\,(\text{eV Å}^3)^{-1}$. The color scale is black → red → yellow and corresponds to a corrugation of 1.5 Å.

We calculate NO adsorption energies using the following equation:

$$\Delta E_{ads} = E(n \cdot NO/Mo_xS_y) - E(Mo_xS_y) - n \cdot E(NO(g)) \qquad (1)$$

$E(n \cdot NO/Mo_xS_y)$ is the energy of the edge structure with n bound NO molecules per unit cell, $E(Mo_xS_y)$ is the energy of the edge structure, and $E(NO(g))$ is the energy of one NO molecule in the gas phase.

Likewise, we calculate vacancy formation energies, as e.g. for the energy of for creating n vacancies per unit cell

$$\Delta E_{vac} = E(Mo_xS_{y-n}) + n \cdot E(H_2S(g)) - E(Mo_xS_y) - n \cdot E(H_2(g)) \qquad (2)$$

where $E(Mo_xS_{y-n})$ is the energy of the edge structure where nS atom have been removed per unit cell, $E(H_2S(g))$ is the energy of H$_2$S in the gas phase and $E(H_2(g))$ is the energy of H$_2$ in the gas phase. We also calculate the combined adsorption and vacancy formation energies, i.e. we consider a reaction where NO is adsorbed and a vacancy is created at the same time. Combined adsorption and vacancy formation energies are calculated as e.g. the adsorption of one NO molecule and the creation of one vacancy:

$$\Delta E_{ads+vac} = E(NO/Mo_xS_{y-1}) + E(H_2S(g)) - E(Mo_xS_y)$$
$$- E(H_2(g)) - E(NO(g)) \qquad (3)$$

Here, $E(NO/Mo_xS_{y-1})$ is the energy of an edge structure, where one S atom has been removed and NO has been adsorbed instead.

3. Results and discussions

Fig. 4 shows the IR spectrum for the unpromoted MoS$_2$ catalyst after NO adsorption, which is the starting point for our studies. As reported earlier by Topsøe et al. [18], the adsorption of NO on a sulfided Mo/Al$_2$O$_3$ gives rise to two main IR absorption bands at 1786 cm^{-1} and 1699 cm^{-1}. The adsorption sites for NO were originally interpreted as vacancies created upon evacuation after sulfidation [18]. Based on comparison with various adsorption complexes and metal cluster complexes [18], the two absorption bands were assigned to the symmetric and asymmetric stretching vibrations of dinitrosyl or dimeric species adsorbed on Mo site at the edges of MoS$_2$ slabs. However, direct evidence for the adsorption configuration and binding site of NO as well as an understanding of the adsorption mechanism has been missing.

3.1. NO adsorption on MoS$_2$ observed by STM

To achieve a fundamental atomic-scale understanding on the interaction between NO and the single-layer MoS$_2$ nanoclusters and to address the issue whether NO observed in the experiments preferentially adsorbs as mono-or dinitrosyls, we have performed STM experiments on a model system consisting of fully sulfided

MoS$_2$ nanoclusters supported on the Au substrate. Our previous STM studies have shown that MoS$_2$ nanoclusters synthesized in a pure H$_2$S atmosphere adopt a triangular morphology, exposing exclusively the (10$\bar{1}$0) Mo-edges, which are fully sulfided and terminated by sulfur dimers (Fig. 3). The main STM signatures of this Mo-edge have been thoroughly analyzed and understood in previous studies [56, 57, 63, 66] and by comparing the appearance before and after NO exposure, we can image the effects of NO adsorption on the atomic scale. Upon dosing NO onto the freshly synthesized MoS$_2$ nanoclusters, no changes in the atom-resolved STM images of the MoS$_2$ structure – neither on the edge nor on the basal plane positions – can be observed. This means that NO does not adsorb on the fully sulfided Mo-edge terminated by sulfur dimers. To confirm this, we calculate NO adsorption on the Mo-edge terminated with sulfur dimers (see Supporting information, configuration 17Mo) and find that NO spontaneously desorbs during structural relaxation and ends up several Ångstroms above the surface with endothermic adsorption energy of 29 kJ/mol. This result is not surprising and suggests that coordinatively unsaturated sites may be necessary for adsorption of NO at the edge. In order to test this, STM experiments were carried out with MoS$_2$ nanoclusters activated by treatment with pre-dissociated hydrogen, since previous studies have shown that this may lead to the creation of sulfur vacancies at the edges of the clusters [61,80]. The atom-resolved STM images in Fig. 5a and b shows the MoS$_2$ nanoclusters after such exposure to atomic hydrogen and subsequent dosing of NO. Marked with white arrows in Fig. 5a and b, the STM images clearly show a number of very bright atom-sized protrusions located at the edges of the MoS$_2$ nanoclusters. An accompanying feature is a slight depletion of the bright brim located adjacent to the unperturbed Mo-edge of the clean MoS$_2$ nanocluster [66]. Similar types of features were not observed on neither the clean nor the atomic hydrogen-dosed MoS$_2$ nanoclusters. In contrast, the sulfur vacancies revealed in previous STM studies [56,71,85] were imaged as dark depletions on the edge sulfur positions. Therefore, the new bright protrusions observed in the STM images are attributed to NO molecules adsorbed at the edges of the clusters. Interestingly, the adsorbed NO nearly always appears in pairs, with the protrusions separated by a spacing of 3.2 Å in the direction parallel to the edge, which is very close to the normal distance of 3.15 Å between Mo atoms on the clean Mo-edge (see line scan in Fig. 6c). Although single NO species also could be observed, the pairwise configuration must be a particularly stable configuration based on its high abundance.

In order to elucidate the nature and adsorption configuration of NO, a close-up image of the NO pair with the structure of MoS$_2$ embedded in the STM image is analyzed in Fig. 6a. The image reveals that the two bright protrusions contained in the NO pair are both located at the Mo-edge atoms on the same position as the original sulfur dimers (Fig. 3). Further insight into the exact structure is obtained from DFT calculations. We have calculated a wide range of adsorption geometries of both mononitrosyl and dinitrosyl structures on the Mo-edge surrounded by sulfur dimers (Table 2 in the Supporting information) and compared the simulated STM images to the experimental ones (see Table 3 in the Supporting information for all simulated STM images). Among all configurations, number 24Mo, a pair of dinitrosyls, provides the best match to experiments both in terms of a reasonable value for the combined vacancy creation and NO adsorption energy $\Delta E_{ads+vac}$ and in terms of agreement between the simulated and the experimental STM images. A structural model of the 24Mo configuration is depicted in Fig. 6d. In this favorable configuration, the NO probe molecules are seen to adsorb as dinitrosyl pairs surrounded by sulfur dimers. The simulated STM image (Fig. 6b) of the 24Mo structure reproduces both the bright protrusions located on the original positions of the sulfur atoms at the edge as well as
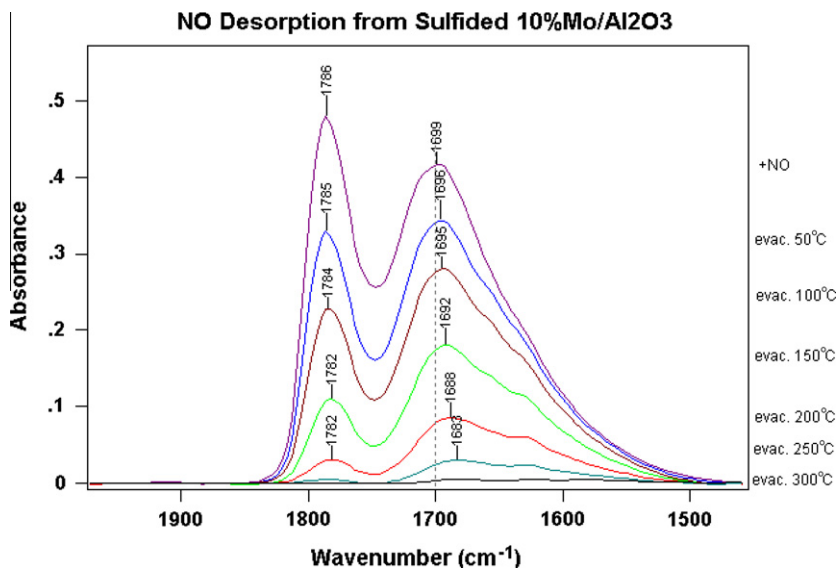
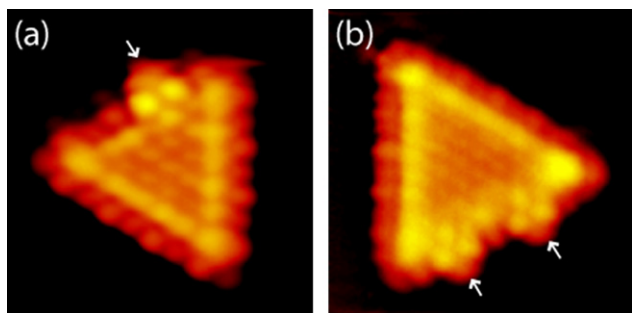Fig. 4. IR spectra of NO desorbed from a sulfided 10% Mo/Al$_2$O$_3$ via evacuation at different temperatures.

Fig. 5. (a) and (b) STM images of MoS$_2$ nanoclusters after exposure to atomic hydrogen and subsequent exposure to NO. Images are 34 × 34 Å^2 and 47 × 47 Å^2 and the tunneling parameters are I_t = 0.8 nA and V_t = −0.1 V. The arrows mark the position of the adsorbed NO pairs.

the slight depletion of the bright brim structure located one atomic row further back. None of the other calculated structures shows a simulated STM image with protrusions and depletions at the same atomic positions as the experimental one. In support of this config- uration, DFT results show that there is a strong preference to form a neighboring dinitrosyl pair compared to two dinitrosyls sepa- rated by one or more sulfur dimers, which is calculated to be unfa- vorable by 109 kJ/mol. This strong preference can be explained by the fact that the sulfur dimers at the edge have also shown to ex- hibit an energetically favorable pairing along the edge [57,59], i.e. in the x-direction (see Fig. 3). Therefore, once one NO is adsorbed and replaces a sulfur dimer, it is more favorable to adsorb NO and replace a sulfur dimer right next to it compared to a situation where the dinitrosyl group is located further apart. In general, one may have a situation, where the Au substrate may influence the STM image of the MoS$_2$ clusters and the agreement between observed and simulated STM images may not be that good unless
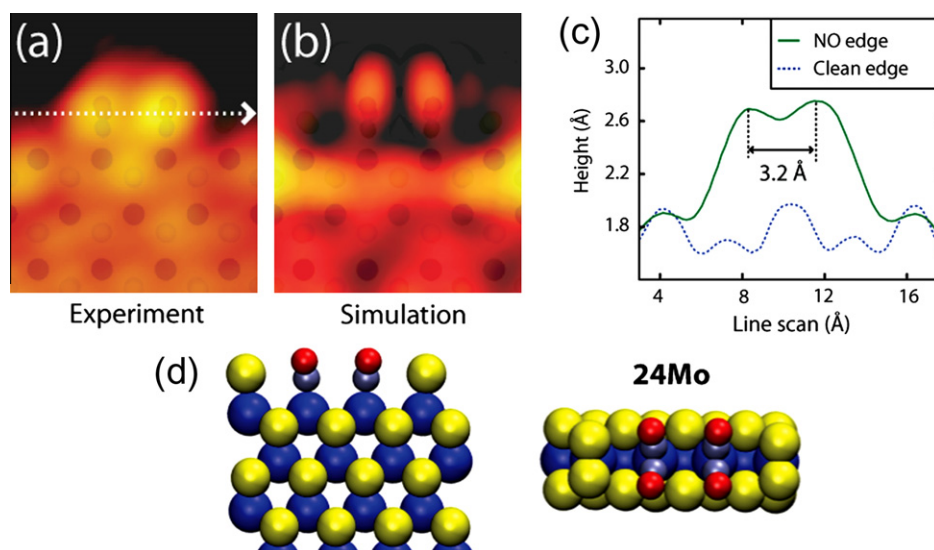

Fig. 6. (a) Close-up image of a NO pair adsorbed on the Mo-edge of an MoS$_2$ nanocluster and (b) STM simulation of configuration **24Mo** (see Supplementary information) consisting of two neighboring dinitrosyl groups adsorbed on the Mo-edge and including the Au support. Both images are embedded with a ball model of configuration **24Mo**. (c) STM linescan over the NO pair. The position of the linescan is indicated in (a). For reference a clean edge without NO adsorbates is included. (d) Ball model (top view and side view) of configuration **24Mo**.
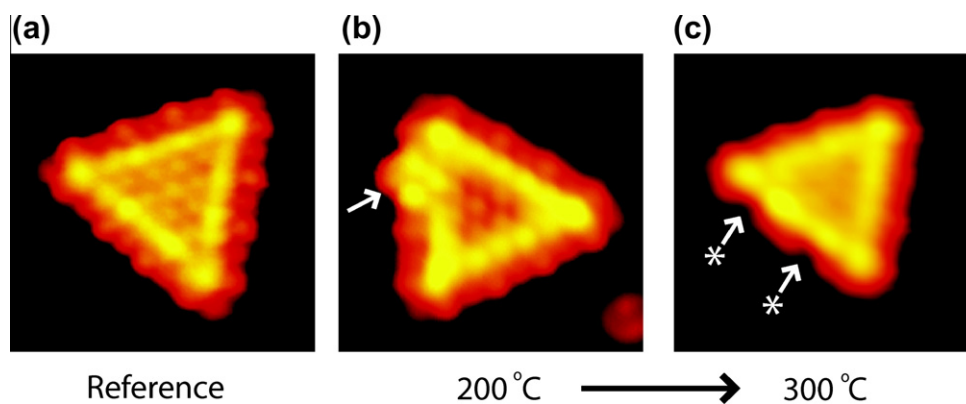
Fig. 7. NO desorption experiments. (a) A reference STM image of a clean MoS_2 nanoclusters exposing fully sulfided edges. (b) STM images showing clusters after exposure to atomic hydrogen and NO and subsequent annealing to 200 °C. (c) Similar clusters after annealing to 300 °C. All images are 35×35 Å^2 and the tunneling parameters are $I_t = 0.6$ nA and $V_t = -0.3$ V. White arrows mark the position of NO pairs while * mark the position of sulfur vacancies.

the Au substrate is taken into account in the DFT calculations. Therefore, we have investigated the influence of the Au substrate on the simulated STM images extensively in this study (see Supporting information). However, we find the effect of the Au substrate on the simulated STM images to be negligible (note that Fig. 6b is a simulation that includes the Au substrate).

From the STM experiments, it is also possible to investigate the desorption process of NO and get an estimate of the binding strength of the NO pairs by successively heating to higher temperature and recording the temperature at which the NO molecules have desorbed (similar to temperature-programmed desorption, TPD). Fig. 7 shows such atom-resolved STM images obtained after annealing to 200 °C and 300 °C together with a reference image of a clean MoS_2 nanocluster. The STM image in Fig. 7b clearly shows that the NO pairs are still present in the same dinitrosyl configuration as at room temperature (cf. Fig. 5) after heating to 200 °C. Upon heating to 300 °C, however, the NO molecules disappear from the edges as illustrated in Fig. 7c. These temperatures correspond well to the desorption temperatures measured in TPD experiments by Okamoto et al. [96] and the present IR-TPD results. The STM image in Fig. 7c reveals that two sulfur vacancies marked by arrows are present at the edges after desorption of the NO molecules. This is reasonable since no H_2S is present to fill these vacancies under UHV conditions, which again supports the conclusion that sulfur vacancies were the original adsorption sites on the MoS_2 edge. It should be noted that after treatment with atomic hydrogen, one may besides vacancies also produce S–H groups. Thus, some NO adsorption may also occur via the push–pull mechanism discussed in Sections 2.3. and 3.2. However, the conclusions regarding the structure of the final adsorption complex will not be influenced by this. After desorption, the two S vacancies in the STM image are spaced several atomic distances apart, which is tentatively attributed to vacancy mobility at elevated temperature. Previously, it has been speculated that NO adsorption on MoS_2 may result in decomposition of NO and oxidation of the MoS_2 edges. The resemblance of the sulfur vacancies observed in Fig. 7c with those observed before NO exposure [85] shows clearly that NO dosing does not lead to oxidation of the edges.

3.2. Mechanism of NO adsorption

Under HDS conditions, the MoS_2 nanoclusters are exposed to a much higher hydrogen pressure than under the model STM studies. However, it is now rather well understood, how the general MoS_2 morphology, the atomic edge structure and the sulfur and hydrogen coverages of the edges depend closely on the surrounding gas atmosphere [60,66,68]. Under typical industrial HDS conditions, MoS_2 nanoclusters adopt a hexagonal shape exposing both low-index edges, the $(1\,0\,\bar{1}\,0)$ Mo-edge and the $(\bar{1}\,0\,1\,0)$ S-edge, according to previous experimental results [60] and calculated phase diagrams [66,68]. The Mo-edge is terminated by sulfur monomers with a partial hydrogen coverage, whereas the S-edge is found to be saturated with sulfur dimers with adsorbed hydrogen [57,60,74] (see Fig. 3). To understand NO adsorption at all the relevant edges, we have calculated NO adsorption at the edge terminations exposed to both the sulfiding STM conditions [56,57] and the hydrogen-rich conditions used during sulfiding in the IR experiments with a hydrogen-sulfur ratio of $H_2/H_2S = 50$, which resembles HDS conditions [60,77,78]. Tables 1 and 2 list the most relevant structures for the following analysis. The remaining structures are documented in the Supporting information.

Before continuing with the detailed discussion of the IR results, it is important to point out that according to the DFT results, the general interaction of NO with edges without sulfur vacancies is very weak, irrespective of the edge type. This is in accordance with the STM results. Even for a reduced, 50% sulfur covered Mo-edge (sulfur monomers in Fig. 3), it is found that NO only adsorbs very weakly with -17 kJ/mol (structure **8Mo** in Table 1). Hence, NO is not expected to be present in this state except maybe physisorbed at very low temperatures. In contrast, the direct NO adsorption (ΔE_{ads}) onto the coordinatively unsaturated Mo atoms at the edges exposing sulfur vacancies is found to be exceedingly exothermic with energies exceeding -500 kJ/mol for the most relevant structures. It is interesting that these energies exceed the otherwise quite large energy needed to form sulfur vacancies [66,77,78] so that the combined vacancy creation and NO adsorption is in overall exothermic. This result shows that a relevant parameter that determines whether NO adsorption can take place is the combined vacancy creation and NO adsorption energy $\Delta E_{ads+vac}$. For example, for the Mo-edge termination with sulfur monomers, which is predicted to be present under HDS conditions (see Fig. 3), the energetically most favorable adsorption configuration is a pair of NO mononitrosyls adsorbed at two Mo-edge sites adjacent to each other (structure **1Mo** in Table 1). The combined vacancy formation and adsorption energy of this configuration is calculated to be $\Delta E_{ads+vac} = -218$ kJ/mol. The very strong adsorption of NO thus indicates that instead of creating a vacancy prior to NO adsorption and subsequently adsorbing NO, it is more likely that these two reactions occur simultaneously via a "push–pull" mechanism where NO replaces the edge S–H groups in a concerted mechanism. Similar findings were also reported by Wen et al. [54, 55] on DFT calculation on a $Mo_{16}S_{32}$ cluster where NO adsorption was found to displace H_2S resulting in adsorbed NO on the Mo-edge stripped

Table 1

Structures, energies and vibrational frequencies for all NO adsorption structures on the unpromoted Mo-edge discussed in the paper. All ID numbers end with Mo, and the number in brackets indicates the number of NO molecules per 2×4 unit cell. Two unit cells in the x-direction are displayed. All energies and frequencies are calculated self-consistently with the RPBE functional, except for frequency values in brackets, which are obtained with the PW91 functional. If there is more than one NO molecule per unit cell, ΔE_{ads} is calculated for adsorption of all NO molecules in the unit cell. The combined vacancy formation and adsorption energies are obtained using the structure present under HDS conditions (terminated by sulfur monomers and 50% H) as reference structure. Symmetric modes are marked with (s) and antisymmetric modes with (a).

ID (number NO)	Adsorption structures	ΔE_{ads} (kJ/mol)	$\Delta E_{ads+vac}$ (kJ/mol)	NO frequencies (cm^{-1})
1Mo (2 NO) (2 NO)		−543	−218	1766 (s), 1679 (a) (PW91: 1775 (s), 1686 (a))
2Mo (1 NO) (1 NO)		−301	+23	1699 (PW91: 1707)
3Mo[a] (4 NO)		−527	−202	1532 (ss), 1530 (as), 1486 (aa), 1469 (sa)[b] (PW91: 1543 (ss), 1539 (as), 1494 (aa), 1478 (sa))
4Mo (2 NO)		−389	−64	1580 (s), 1502 (a) (PW91: 1582 (s), 1507 (a))
5Mo (1 NO)		−260	−98	1666 (PW91: 1664)
6Mo (1 NO)		−137	−74	1727 (PW91: 1735)
7Mo (2 NO)		−150	−87	1499 (s), 1492 (a) (PW91: 1514 (s), 1504 (a))
8Mo (1 NO)		−17	N/A[c]	1754 (PW91: 1694[d])

[a] A structure with dinitrosyls in a bridge coordination between the Mo atoms was also investigated, but relaxed to the **3Mo** structure in the calculation.

[b] Notation is ss: symmetric both within one dinitrosyl and from one to the next, as: antisymmetric within one dinitrosyl, symmetric from one to the next, aa: antisymmetric within one dinitrosyl and antisymmetric from one to the next, sa: symmetric within one dinitrosyl, antisymmetric from one to the next.

[c] Cannot be calculated, as no vacancy is formed upon adsorption.

[d] Relaxes to a slightly different structure in PW91 than in RPBE. This is probably because the NO molecule is so weakly bound.

off sulfur. Without NO adsorption, creation of a completely stripped Mo-edge would be energetically extremely expensive. Thus, in order to find the most stable NO adsorption structure, one has to investigate various adsorption configurations involving different sulfur, hydrogen and NO coverages and compare them with respect to the combined vacancy formation and NO adsorption energy $\Delta E_{ads+vac}$. It should be noted that this combined adsorption and vacancy creation mechanism can only take place when adsorbed hydrogen is available on the edge. Therefore, NO adsorption is not seen in the STM experiments, unless S–H groups are made available on the edges.

In IR experiments on MoS$_2$ catalysts, the presence of S–H groups is also evidenced through the strong hydrogen bonding band observed around 3600 cm^{-1} [97]. Upon NO adsorption, a decrease

Table 2
Structures, energies and vibrational frequencies for the most relevant NO adsorption structures for the unpromoted S-edge discussed in the paper. All ID numbers end with S, and the number in brackets indicates the number of NO molecules per 2×4 unit cell. Two unit cells in the x-direction are displayed. All energies and frequencies are calculated self-consistently with the RPBE functional, except for frequency values in brackets, which are obtained with the PW91 functional. If there is more than one NO molecule per unit cell, ΔE_{ads} is calculated for adsorption of all NO molecules in the unit cell. The combined vacancy formation and adsorption energies are obtained using the structure present under HDS conditions (sulfur dimers that are fully covered with H) as reference structure.

ID (number NO)	Adsorption structures	ΔE_{ads} (kJ/mol)	$\Delta E_{ads+vac}$ (kJ/mol)	NO frequencies (cm^{-1})
1S (4 NO)		−819	−226	1817 (ss), 1781 (as), 1745 (sa), 1706 (aa)[a] (PW91: 1825 (ss), 1789 (as), 1753 (sa), 1713 (aa))
2S (2 NO)		−480	113	1725 (s), 1687 (a) (PW91: 1738 (s), 1700 (a))
3S (2NO)		−580	14	1526, 1278 (PW91: 1544, 1279)
4S (2NO)		−221	−81	1766 (s), 1762 (a) (PW91: 1773 (s), 1770 (a))
5S (1NO)		−98	41	1757 (PW91: 1767)

[a] Notation is ss: symmetric both within one dinitrosyl and from one to the next, as: antisymmetric within one dinitrosyl, symmetric from one to the next, sa: symmetric within one dinitrosyl, antisymmetric from one to the next, aa: antisymmetric within one dinitrosyl and antisymmetric from one to the next.

in the extent of hydrogen bonding is usually observed. This supports that the NO adsorption occurs via a push–pull mechanism, since the concentration of S–H groups is reduced.

Since all the catalysts used in the IR studies are supported on alumina, it is relevant to briefly discuss support interactions. It is well known that type I catalysts with Al–O–Mo linkages between the MoS$_2$ structures and the support are less active than type II structures without those linkages [2,98]. Previous studies have used DFT to gain insight into support interactions, either by modeling type I sites by simple Mo–O–Al linkages [72,99] or by considering full alumina and titania substrates [100,101,102]. We have demonstrated in a previous DFT study of type I/type II structures that if these linkages are present, their influence is quite local, i.e. they may affect the sites right next to them, but sites a few lattice spacings away are unaffected. So the presence of type I sites in the catalyst may have a limited influence on type II active sites further away. In a previous IR study of NO adsorption on type I and type II Co–Mo–S structures [44], no large changes in band positions were observed. Thus, this suggests that the models used in the DFT calculations are relevant for interpreting the results on alumina-supported catalysts.
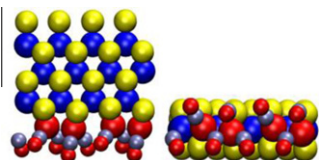
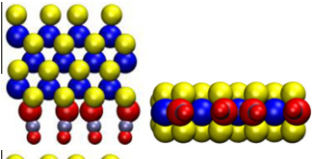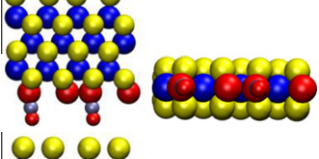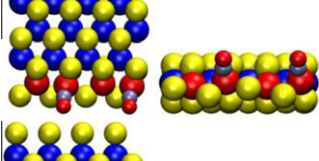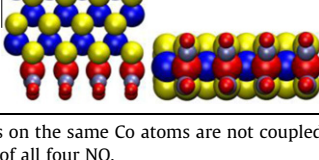## 3.3. Comparison of IR and DFT results

The NO adsorption bands observed in the IR spectra in Fig. 4 are generally quite broad, especially the lower frequency band [18]. The broadness indicates that several adsorption complexes exist. To elucidate the detailed nature of the NO adsorption and

evaluate the relative adsorption strength of these different species, we analyze spectra after desorption of NO at progressively increasing temperatures. The IR spectra recorded in this manner (Fig. 4) reveal changes in the relative intensity of the two bands upon desorption. This TPD analysis confirms that the complex structure of the IR peaks cannot arise solely from a single dinitrosyl or dimeric species, but more likely must be associated with several nitrosyl species with different binding strengths. In the following, these experimental results are compared to the structures and corresponding energies and vibrational frequencies calculated from DFT.

3.3.1. NO adsorption at the unpromoted Mo-edge

The vibrational frequencies for the previously discussed most stable adsorption configuration for NO at the Mo-edge (structure **1Mo** in Table 1) are calculated to be 1766 cm^{-1} and 1679 cm^{-1} for the symmetric and asymmetric stretching modes, respectively, for the NO pairs on the fully substituted edge. The calculated frequencies are in good agreement with the two peaks at 1786 cm^{-1} and 1699 cm^{-1} observed by IR at high NO coverage (Fig. 4). In contrast, the calculated frequencies for the slightly less stable dinitrosyl pairs (structure **3Mo**) are in the range of 1469–1532 cm^{-1}. Experimentally, no distinct peaks in this region are observed, and therefore we can exclude the presence of the dinitrosyl structures. It should furthermore be noted that bridge coordination of the mononitrosyls (structure **4Mo**) can also be excluded, since this structure is 154 kJ/mol higher in energy and its vibrational frequencies are much lower than the experimental values.

Table 3

Structures, energies and vibrational frequencies for all NO adsorption structures for the promoted Co–Mo–S-edge discussed in the paper. All ID numbers end with Co, and the number in brackets indicates the number of NO molecules per 2×4 unit cell. Two unit cells in the x-direction are displayed. All energies and frequencies are calculated self-consistently with the RPBE functional, except for frequency values in brackets, which are obtained with the PW91 functional. If there is more than one NO molecule per unit cell, ΔE_{ads} is calculated for adsorption of all NO molecules in the unit cell. The combined vacancy formation and adsorption energies are obtained using the structure present under HDS conditions (sulfur monomers and 50% H) as reference structure.

ID (number NO)	Adsorption structures	ΔE_{ads} (kJ/mol)	$\Delta E_{ads+vac}$ (kJ/mol)	NO frequencies (cm^{-1})
1Co (4 NO)		−650	−338	1814[a], 1774[b], 1701[c], 1600[d] (PW91: 1816[a], 1771[b], 1670[c], 1609[d])
2Co (2 NO)		−514	−201	1827 (s), 1745 (a) (PW91: 1837 (s), 1757 (a))
3Co (1 NO)		−285	28	1772 (PW91: 1790)
4Co (1 NO)		−23	N/A[e]	1865 (PW91: 1874)
5Co (4 NO)		−582	−269	1868[f], 1796[g], 1681[h], 1601[i] (PW91: 1867[f], 1795[g], 1682[h], 1602[i])

Note that the NO pairs on the same Co atoms are not coupled.
[a] Symmetric model of all four NO.
[b] Antisymmetric mode of the left NO pair.
[c] Antisymmetric mode of top right NO weakly coupled to left pair of NO.
[d] Antisymmetric mode of bottom right NO weakly coupled to left pair of NO.
[e] Cannot be calculated, as no vacancy is formed upon adsorption.
[f] Symmetric coupling of the upper NO molecules on different Co atoms.
[g] Antisymmetric coupling of the upper NO molecules on different Co atoms.
[h] Symmetric coupling of the lower NO molecules on different Co atoms.
[i] Antisymmetric coupling of the lower NO molecules on different Co atoms.

It is interesting to note that for mononitrosyls or dinitrosyls separated by a sulfur atom (structures **6Mo** and **7Mo**), the dinitrosyl configuration is slightly more stable by 13 kJ/mol compared to the mononitrosyl configuration. This is in agreement with stabilization of the dinitrosyl structures in the calculations with the 4×4 model for the STM simulations (see Supporting information). However, overall we note that $\Delta E_{ads+vac}$ is significantly lower for structure **1Mo** than for **6Mo** and **7Mo**, meaning that complete substitution of sulfur by NO is expected to prevail, and in this case, mononitrosyl species are again the most stable.

It should be also noticed that in an actual catalyst one will have clusters with different sizes. Thus, the edge length and the fraction of atoms at or close to corners will vary, and this may give rise to **1Mo** species with slightly different frequencies. Such effects are not considered in the present DFT calculations, but are discussed in more detail in Section 3.4 where the present infinite slab calculations are compared to calculations on cluster structures.

When one of the NO molecules is removed from the **1Mo** configuration, the structure **2Mo** in Table 1 is created corresponding to a situation where vacancies and mononitrosyls coexist on the

Mo-edge during desorption at elevated temperatures. This mononitrosyl adsorption species has an adsorption energy of −301 kJ/mol and the corresponding vibrational frequency is calculated to be 1699 cm^{-1}. This is also in excellent agreement with the experimental IR observations shown in Fig. 4. Upon desorption of NO, the relative intensity of the lower frequency band at 1695 cm^{-1} increases compared to the higher frequency band at 1784 cm^{-1} (see Fig. 4). It is also observed that the lower frequency band shifts to slightly lower values (a shift of 14 cm^{-1} downwards upon heating to 300 °C). From the DFT calculations, it is found that the structure **5Mo**, where the Mo-edge is terminated partly with NO and partly with SH groups, is quite stable with NO adsorption energy of −260 kJ/mol and gives rise to a band at 1666 cm^{-1}. It is possible that this structure contributes to the downwards shift observed at elevated temperature in Fig. 4. The similar structure **6Mo** is higher in energy and therefore not expected to be significant.

3.3.2. NO adsorption at the unpromoted S-edge

The S-edge present under HDS conditions, which is terminated by sulfur dimers and one adsorbed hydrogen atom per sulfur dimer
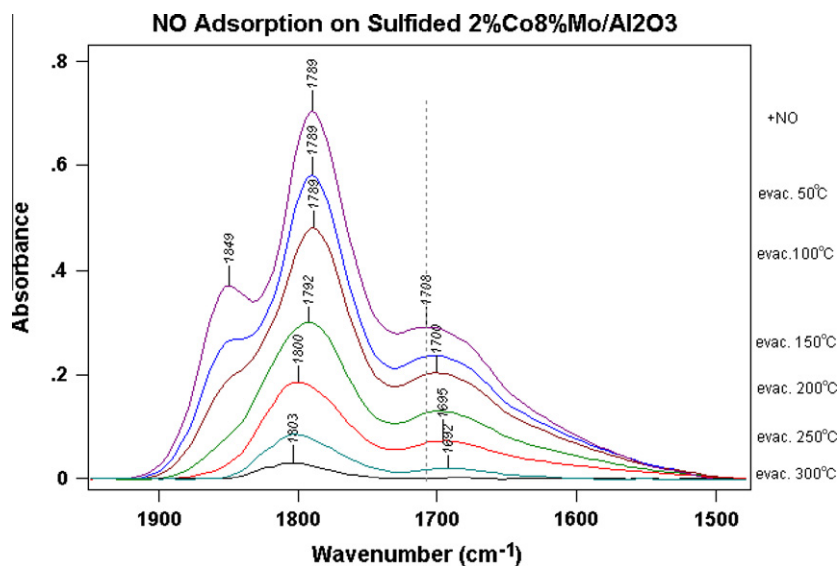
Fig. 8. IR spectra of NO desorbed from a sulfided 2% Co 8% Mo/Al$_2$O$_3$ via evacuation at different temperatures.
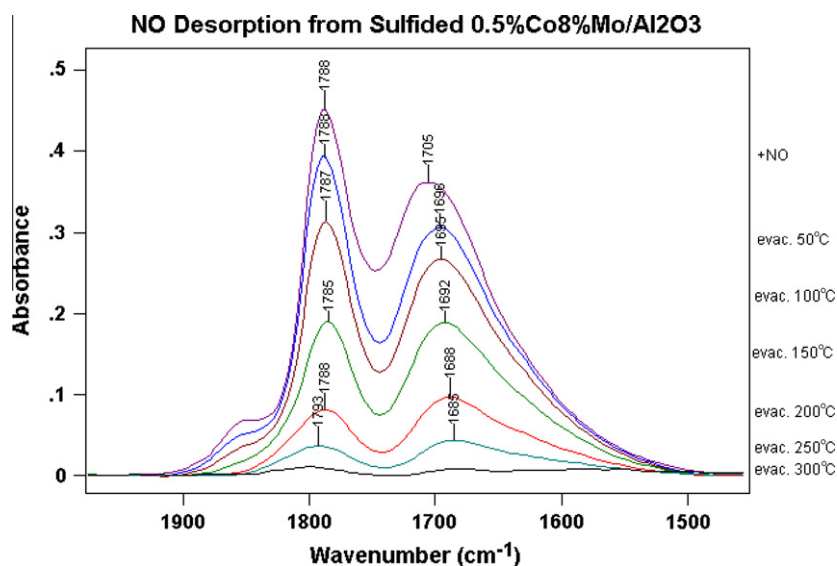

Fig. 9. IR spectra of NO desorbed from a sulfided 0.5% Co 8% Mo/Al$_2$O$_3$ via evacuation at different temperatures.

(see Fig. 3), is presumably inactive toward NO adsorption without simultaneous creation of vacancies. This is in line with the results for the fully sulfided Mo-edge and the general inactivity of this S-edge toward other molecules [77]. Therefore, we proceed along the same lines as for the Mo-edge and investigate NO adsorption configurations for structures with lower sulfur coverages. The most important structures are listed in Table 2, and the remaining structures can be found in the Supporting information. The most stable structure in terms of $\Delta E_{ads+vac}$ is structure **1S** with dinitrosyl species, which has an adsorption energy of −819 kJ/mol and gives rise to NO absorption band frequencies at 1817, 1781, 1745, and 1706 cm^{-1}. We also find a stable mononitrosyl structure **4S**, for which sulfur monomers are still present. This structure has an adsorption energy of −221 kJ/mol and gives rise to the frequencies 1766 cm^{-1} and 1762 cm^{-1}, two almost degenerate modes. Even though the mononitrosyl structure is energetically less stable ($\Delta E_{ads+vac}$), one could imagine it to be present when substitution of S by NO is incomplete. A comparison with the IR spectra of NO

adsorbed on alumina-supported MoS$_2$ catalyst shows indeed that all these energetically favorable NO adsorption modes found from DFT calculations have vibrational frequencies lying within the observed range.

On the S-edge, upon removal of one NO from each dinitrosyl during the desorption process, we find two different structures, the more stable 3**S** structure with adsorption energy of −580 kJ/mol and NO band frequencies of 1278 cm^{-1} and 1526 cm^{-1} and the less stable 2**S** structure with adsorption energy of −480 kJ/mol and NO band frequencies of 1725 cm^{-1} and 1687 cm^{-1}. It is, however, questionable whether the structures 2**S** or 3**S** will occur upon desorption of NO, or whether some sulfur will readsorb due to the presence of some H$_2$S in the gas phase and structure 4**S** may thus be present.

To summarize, we find that the observed IR spectra consist of contributions from NO adsorbed at both the Mo-edge and the S-edge. As already discussed earlier, the IR spectrum at room temperature shows a higher frequency band at 1786 cm^{-1} and a rather

broad lower frequency band at 1699 cm^{-1}. Upon desorption at elevated temperatures, the intensity of the higher frequency band is seen to decrease faster than that of the lower frequency band. Beside this, downward shifts are also observed in both IR absorption bands. From DFT calculations, the adsorption structures **1Mo** and **1S** were found depicting NO adsorbed as mononitrosyl at the Mo-edge and as dinitrosyl at the S-edge, respectively, leading to various NO absorption bands in the frequency range of 1817 cm^{-1} to 1679 cm^{-1}. Upon removal of one of the NO molecules from the NO pair, the configurations **2S** and **3S** described earlier are in good agreement with the experimental observation in that absorption bands at lower frequency dominate in the structures. Also, the calculated frequencies of the **4S** structure are in good agreement with experiments. The result that upon desorption the structure formed at the S-edge has a larger desorption energy (580 kJ/mol) when compared to that at the Mo-edge (301 kJ/mol) indicates that NO adsorbs stronger at the S-edge. Thus, one would expect the former configurations **2S** and **3S** to predominate at the highest temperature during the desorption experiment, but **4S** may also be present. The lower frequency calculated for these structures is consistent with the IR observation where a significant downward shift is observed in the low-frequency NO band.

3.3.3. NO adsorption on the promoted Co–Mo–S-edge

STM experiments and DFT calculations have previously shown that Co-promoted MoS$_2$ nanoclusters (Co–Mo–S) adopt a hexagonal shape terminated by the unpromoted Mo-edges (like the unpromoted case previously discussed) and Co-promoted S-edges (termed Co–Mo–S-edges) with the Co promoter atom replacing Mo [58,62,71] (see Fig. 3 for the structure of the Co–Mo–S-edge under hydrotreating conditions). Co incorporation at the Mo-edge has never been directly observed in our STM experiments, and therefore we consider in the present study Co to be incorporated on the S-edge only.

The promoting role of Co is uniquely linked to the formation of the Co–Mo–S-edges, and it is therefore relevant to clarify the nature of NO as a probe molecule for the promoted phase. As Co is favored to promote the S-edge, a study of different promoted catalysts will simultaneously allow us to get information on the relative abundance of promoted S-edges, unpromoted Mo-edges, and unpromoted S-edges. Information on the presence of unpromoted S-edges is interesting, since in optimally promoted catalysts the concentration of such edges should be low. In order to illustrate this point, the results for two MoS$_2$ catalysts promoted with 2% and 0.5% Co, respectively, will be discussed. These catalysts were prepared such that for the 2% Co all the available S-edge sites of the MoS$_2$ should be covered. The 0.5% Co sample has a lower activity. Therefore, presumably only a small fraction of the S-edge is covered, and it is expected that some unpromoted S-edge sites are also exposed. Thus, we expect to see NO interact predominately with the Mo-edge and Co–Mo–S-edge in the higher Co-loading catalyst, whereas interaction with both Mo- and unpromoted S-edges are also possible in the catalyst with lower Co concentration.

For the 2% Co-promoted catalyst, three IR absorption bands are observed in the IR spectrum (Fig. 8), which again suggests that several adsorption configurations of NO are present. Furthermore, a series of NO desorption spectra for this catalyst is depicted in Fig. 8. As reported previously [18], the highest frequency band at 1849 cm^{-1} has been attributed to NO adsorbed on Co, while the lowest frequency band at 1708 cm^{-1} is attributed to NO adsorbed on Mo, whereas the band in the middle at 1789 cm^{-1} consists of an overlap of band contributions from NO adsorbed on both Mo and Co. Since most of the S-edge sites in this promoted catalyst are likely to be associated with Co, the lowest frequency band at 1708 cm^{-1} can be assigned to NO adsorbed at Mo-edge, corresponding to structure **1Mo**. The band at 1849 cm^{-1} is not present

in the IR spectra of the unpromoted catalyst (Fig. 4) and must therefore arise from NO adsorption at the Co–Mo–S-edge. Along the same line as for the unpromoted edges, structures with different sulfur and NO coverages were calculated by DFT, and together with the IR-TPD results this allows for a more detailed understanding of NO adsorption. Table 3 enumerates the most relevant structures, and the remaining structures are documented in the Supporting information. The most stable structure **1Co** consists of dinitrosyl species coordinated to the Co atoms. The most stable structure involving mononitrosyl species is **2Co**. Both structures give rise to a series of vibrational bands with frequencies ranging from 1827 cm^{-1} to 1600 cm^{-1}. This range is consistent with the experimentally observed frequencies. However, it should be noticed that also the structure **4Co** with weakly adsorbed NO might contribute to the higher-lying band. However, this contribution should vanish rapidly upon heating, which is not the case as seen in Fig. 8, and therefore, we assign the band at 1849 cm^{-1} to arise from both dinitrosyl and mononitrosyl species **1Co** and **2Co**.

From Fig. 8, it is evident that upon desorption at increasing temperature, the species associated with the highest frequency band at 1849 cm^{-1} desorb most readily while the middle band at 1789 cm^{-1} disappears most slowly accompanied by a significant upward frequency shift (an upward shift of 14 cm^{-1} from room temperature to 300°C). In contrast, the corresponding band at 1786 cm^{-1} at the unpromoted Mo/Al$_2$O$_3$ catalyst (see Fig. 4) exhibits only a slight downward shift of 6 cm^{-1}. In order to reflect the desorption process, one NO molecule has been removed from each second mononitrosyl in structure **2Co**. The resulting structure **3Co** shows only a single band at 1772 cm^{-1}. This is in excellent agreement with the IR observations where the highest frequency band disappears first upon desorption. Furthermore, this result shows that the middle band most likely arises from NO adsorbed on Co–Mo–S-edge site. It is also noted that after high-temperature desorption, the low-frequency band at 1692 cm^{-1} in the Co-Mo–S catalyst has a slightly higher frequency than the low-frequency band from the unpromoted catalyst at 1683 cm^{-1}. This can be understood considering that for the Co–Mo–S catalyst this band arises mainly from NO adsorbed at the unpromoted Mo-edge (structure **2Mo** with frequency 1699 cm^{-1}). In contrast, for the unpromoted catalyst both the structure **2Mo** and the structure with NO adsorbed at the unpromoted S-edge (structure **2S** with frequencies 1725 cm^{-1} and 1687 cm^{-1}) would be expected to contribute, since NO binds stronger on the S-edge than on the Mo-edge. It can therefore be concluded from the above results for the 2% Co-promoted catalyst that all the S-edges are promoted and that therefore only unpromoted Mo-edges and promoted S-edges are exposed.

To further confirm our assignment of the NO bands, it is interesting to compare the results for the 2% Co-promoted catalysts from Fig. 8 with the NO adsorption results on a MoS$_2$ catalyst with only a small amount of Co (0.5%) added. The NO adsorption and desorption spectra for this catalyst are shown in Fig. 9. They appear to be rather similar to the spectra for the unpromoted Mo/Al$_2$O$_3$ catalyst (Fig. 4), except that the 0.5% Co catalyst shows a slight upward shift of 5 cm^{-1} in the middle band upon heating and evacuation. This small band toward high frequencies is attributed to the small amount of Co promoter. Furthermore, as for the MoS$_2$ catalyst, a very large downward shift is observed after high-temperature desorption, which confirms that the absorption band remained at this temperature is associated with mostly NO adsorbed at the S-edge. Thus, in contrast to the catalyst with the higher Co loading, this result clearly shows that the small amount of Co promoter atoms has only covered a fraction of the available S-edge sites in this sample. Thus, this catalyst exposes promoted Co–Mo–S-edge sites, unpromoted S-edge sites and unpromoted Mo-edges.

In most catalyst development studies, the NO adsorption technique has mainly been used to get information on the changes in concentration of promoter sites, since their concentrations show quite good correlations with the catalytic activities (Figs. 1 and 2). In this way, it has been possible to get insight into how precursor structures, deactivation and other preparation parameters influence activity. Naturally, if deposits block the different edges, the nature of the correlations may change. The present results on the catalysts with different Co loadings show that besides getting information on the promoter sites, one can obtain more information on the nature of the unpromoted sites and to what extend further promotion of these can be achieved. This insight may also contribute to understanding the selectivities of different promoted catalysts. In the future, it would also be very interesting to conduct a similar investigation for Ni–Mo–S catalysts. In contrast to Co, Ni has been observed incorporated into both the Mo- and the S-edge, so the NO adsorption spectrum presumably is a more complicated convolution of unpromoted and promoted sites on both edges.

3.4. Comparison to previous theoretical studies of NO adsorption on MoS₂

It is interesting to compare our results to the results by Wen et al. [54,55] who studied NO adsorption on cluster models. Cluster models give information on NO adsorption close to corner sites, whereas the periodic stripe model probes NO adsorption on the majority of the edge sites in larger nanoclusters far removed from corners. Wen et al. considered hexagonal clusters exposing edges with a width of three Mo atoms ($Mo_{16}S_{32}$, $Mo_{16}S_{34}$ and $Mo_{16}S_{29}$) and Mo-edges with either 0% or 50% sulfur termination and S-edges with 50% or 100% sulfur termination [54]. They also studied a triangular $Mo_{28}S_{60}$ cluster, which exposes Mo-edges with a width of seven Mo atoms and with 50% sulfur termination [55]. Despite the difference in models, there are a number of prominent similarities between the results for MoS₂ in the present study and those from Wen et al. In both studies, frequencies arising from NO coordinated in a bridged position between two Mo atoms tend to be around or smaller than 1600 cm⁻¹ and thereby much smaller than the experimentally observed NO modes. For the Mo-edge, Wen et al. found structures with NO coordinated end-onto one Mo (their structures **2**, **3**, **20–24** in [54]) to be both energetically favorable and their NO vibrational bands to be in agreement with the two observed peaks of 1786 cm⁻¹ and 1699 cm⁻¹ (and the similar results reported by Valyon et al. [19,20]). Their results are in agreement with the present findings for the similar structure **1Mo**. However, in contrast to Wen et al., who found dinitrosyls adsorbed at corners to be stable and their frequencies to be in agreement with experiment (their structures **11**, **12**, **18** in [54]) we find that they are not stable for complete edge substitution (structure **3Mo**) and that their frequencies are lower than those observed. This discrepancy suggests that dinitrosyl structures could be present at Mo-edge corner sites or other isolated sites, but not at edge sites removed from the corners. In this context, it is an interesting question how much corner sites contribute to the IR intensities compared to edge sites. This will be addressed in future studies, which will require information on cluster sizes on the catalysts used in the IR studies. Interestingly, we have recently by STM revealed unique and very interesting reactivity at corner sites for very small activated MoS₂ nanoclusters [85].

For the unpromoted S-edge, we can also compare our results to Wen et al. Since they only investigated the S-edge terminated by sulfur monomers, the structure with adsorbed dinitrosyls **11S** from this study was not identified. For the structures with sulfur monomers and mononitrosyls, however, a number of similarities are noted. Wen et al.'s structure **32** [54] resembles both in structure and in frequency our structure **5S**, in which NO is coordinated

end-onto a Mo atom and the sulfur monomers tend to move away from the adsorbed NO. Furthermore, both studies exclude bridging coordinations, since these adsorption configurations at the S-edge give rise to frequencies which are much lower than those observed. In conclusion, cluster studies [54,55] and the present study using an infinite stripe agree on a number of general issues. This suggests that a number of structural prototypes, e.g. mononitrosyls coordinated end-onto Mo at the Mo-edge, give rise to the observed IR spectra. As these prototypes can occur in different environment, e.g. sites close to the corner sites, sites removed from the corners and sites with different sulfur coordination of neighboring sites, they will give rise to slightly different frequencies (e.g. compare our structures **2Mo**, **5Mo**, **6Mo**). Thus, these different modes are likely the origin of the broad IR bands. At the present time, there are no similar DFT calculations available for promoted systems, but such results may supplement the present results and provide insight into corner effects in promoted systems.

4. Conclusions and outlook

From the interplay of STM, IR and DFT, detailed atomic-scale insight into the adsorption of NO on both unpromoted and Co-promoted MoS₂-based catalysts has been obtained. In general, it is found that on all edges of MoS₂ or Co–Mo–S, NO adsorbs weakly on fully sulfur covered edges not containing hydrogen. The DFT results show that if sulfur vacancies can be formed, these have a big affinity toward adsorption of NO. However, the DFT results also show that it is energetically very unfavorable to create sulfur vacancies and they are therefore not present in any significant amount in the catalysts used for NO adsorption and IR measurements. Nevertheless, NO adsorption readily takes place on such samples and we find that the adsorption on those occurs via a push–pull type mechanism involving simultaneous vacancy creation, adsorption of NO and release of H₂S. This process is overall exothermic.

Generally, the most stable adsorption structures are found to be those where NO has displaced all the sulfur at the edge and adsorbs at every edge site. The rather complex features observed in the IR-TPD spectra can be fully explained by the existence of NO adsorbed in several configurations, dominated by mononitrosyl species at the Mo-edge and dinitrosyls at the S-edge. The above assignment is confirmed by studies of Co-promoted catalysts with varying degrees of promotion. These studies also show that in real industrial Co-promoted catalysts, the Co promoter atoms occupy predominantly the S-edges. Based on the new insight, more information can be derived from IR experiments on promoted catalysts. For example, the results provide insight into the relative concentration of unpromoted Mo-edge sites and the extent to which the S-edges have been promoted. This is important insight, since it gives information on the efficiency of a given preparation process and the potential for further promotion. Regarding the details of the adsorption on the Co–Mo–S-edge, we find that a dinitrosyl species is the most stable structure, but also mononitrosyl structures seem to be possible.

An important remaining question is whether the energy barriers for the reaction pathway of simultaneous sulfur displacement and NO adsorption are such that the push–pull reaction is possible at all temperatures. For CO adsorption, this question has been addressed in cluster calculations [50] and reaction barriers were found to be moderate. As NO adsorption is observed at very low temperatures, one would expect the activation energy for the push–pull mechanism to be quite low as well, but direct calculations need to be addressed in future DFT studies.

Finally, it should also be remarked that support effects have not been addressed in the present study, apart from the investigation

of the influence of the Au support used in the STM studies of MoS$_2$ nanoclusters. Although results in the literature [44] indicate that frequency shifts between type I and type II structures are small, it is expected that NO adsorption will be affected by support interactions, and this will be an important topic for future studies.

Acknowledgments

Appendix A. Supplementary material

Supplementary data associated with this article can be found, in the online version, at doi:10.1016/j.jcat.2011.02.002.

References

[1] A. Stanislaus, A. Marafi, M.S. Rana, Catal. Today 153 (2010) 1.
[2] H. Topsøe, B.S. Clausen, F.E. Massoth, Hydrotreating Catalysis, Springer Verlag, Berlin, 1996.
[3] K.G. Knudsen, B.H. Cooper, H. Topsøe, Appl. Catal. A Gen. 189 (1999) 205.
[4] C. Song, Catal. Today 86 (2003) 211.
[5] M.V. Landau, Catal. Today 36 (1997) 393.
[6] I.V. Babich, J.A. Moulijn, Fuel 82 (2003) 607.
[7] T. Kabe, A. Ishihara, W. Quian, Hydrodesulfurization and Hydrogenation, Wiley-CH, Kodanska, 1999.
[8] R.G. Leliveld, S.E. Eijsbouts, Catal. Today 130 (2008) 183.
[9] B.C. Gates, H. Topsøe, Polyhedron 16 (1997) 3213.
[10] D.D. Whitehurst, T. Isoda, I. Mochida, Adv. Catal. 42 (1998) 345.
[11] M. Houalla, N.K. Nag, A.V. Sapre, D.H. Broderick, B.C. Gates, AIChE J. 24 (1978) 1015.
[12] M. Houalla, D.H. Broderick, A.V. Sapre, N.K. Nag, V.H.J. de Beer, B.C. Gates, H. Kwart, J. Catal. 61 (1980) 523.
[13] M. Egorova, R. Prins, J. Catal. 225 (2004) 417.
[14] Y. Okamoto, Y. Katoh, Y. Mori, T. Imanaka, S. Teranishi, J. Catal. 70 (1981) 445.
[15] H.J. Jung, J.L. Schmitt, H. Ando, in: H.F. Barry, P.C.H. Mitchell (Eds.), Proceedings of the Climax Fourth International Conferences on Chemistry and Uses of Molybdenum, Climax Molybdenum Company, Ann Arbor, Michigan, 1982, p. 246.
[16] N.-Y. Topsøe, H. Topsøe, J. Catal. 75 (1982) 354.
[17] N.-Y. Topsøe, H. Topsøe, J. Catal. 77 (1982) 293.
[18] N.-Y. Topsøe, H. Topsøe, J. Catal. 84 (1983) 386.
[19] J. Valyon, W.K. Hall, J. Catal. 84 (1983) 216.
[20] J. Valyon, R.L. Schneider, W.K. Hall, J. Catal. 85 (1984) 277.
[21] Z. Shuxian, W.K. Hall, G. Ertl, H. Knözinger, J. Catal. 100 (1986) 167.
[22] N. Koizumi, M. Iijima, S. Kasahara, M. Yamada, Chem. Lett. 9 (1996) 815.
[23] N. Koizumi, M. Iijima, T. Mochizuki, M. Yamada, Stud. Surf. Sci. Catal. 106 (1997) 293.
[24] N. Koizumi, K. Takahasi, M. Yahazaki, M. Yamada, Catal. Today 45 (1998) 313.
[25] M. Yamada, N. Koizumi, M. Yamazaki, Catal. Today 50 (1999) 3.
[26] M. Yamazaki, H. Magara, N. Koizumi, M. Yamada, Stud. Surf. Sci. Catal. 126 (1999) 155.
[27] L.P. Nielsen, L. Ibsen, S.V. Christensen, B.S. Clausen, J. Mol. Catal. A: Chem. 162 (2000) 375.
[28] F. Maugé, J. Lamotte, N.S. Nesterenko, O. Manoilova, A.A. Tsyganenko, Catal. Today 70 (2001) 271.
[29] Y. Okamoto, M. Kawano, T. Kubota, Chem. Commun. (2003) 1086.
[30] Y. Okamoto, T. Kubota, Catal. Today 86 (2003) 31.
[31] Y. Okamoto, M. Kawano, T. Kawabata, T. Kubota, I. Hiromitsu, J. Phys. Chem. B 109 (2005) 288.
[32] N. Koizumi, S. Jung, Y. Hamabe, H. Suzuki, M. Yamada, Catal. Lett. 135 (2010) 175.
[33] J. Bachelier, J.-C. Duchet, D. Cornet, Bull. Soc. Chim. Belg. 90 (1981) 1301.
[34] J.B. Peri, J. Phys. Chem. 86 (1982) 1615.
[35] J. Bachelier, M.J. Tilliette, M. Cornac, J.-C. Duchet, j.-C. Lavalley, D. Cornet, Bull. Soc. Chim. Belg. 93 (1984) 743.
[36] B. Müller, A.D. van Langeveld, J.A. Moulijn, H. Knözinger, J. Phys. Chem. 97 (1993) 9028.
[37] X. Qin, G. Xiexian, R. Prada Silvy, P. Grange, B. Demon, in: Proceedings of the Ninth International Congress on Catalysis, vol. 1, Calgary, Canada, 1988, p. 66.
[38] F. Maugé, J.-C. Lavalley, J. Catal. 69 (1992) 137.
[39] L.P.A.F. Elst, S. Eijsbouts, A.D. van Langeveld, J.A. Moulijn, J. Catal. 196 (2000) 95.
[40] A. Travert, C. Dujardin, F. Maugé, S. Cristol, J.F. Paul, E. Payen, D. Bougeard, Catal. Today 70 (2001) 255.
[41] A. Travert, C. Dujardin, F. Maugé, E. Veilly, S. Cristol, J.-F. Paul, E. Payen, J. Phys. Chem. B 110 (2006) 1261.
[42] C. Dujardin, M.A. Lélias, J. Van Gestel, A. Travert, J.C. Duchet, F. Maugé, Appl. Catal. A: Gen. 322 (2007) 46.
[43] N.-Y. Topsøe, Catal. Today 113 (2006) 58.
[44] N.-Y. Topsøe, H. Topsøe, O. Sørensen, B.S. Clausen, R. Candia, Bull. Soc. Chim. Belg. 93 (1984) 727.
[45] H. Topsøe, R. Candia, N.-Y. Topsøe, B.S. Clausen, Bull. Soc. Chim. Belg. 93 (1984) 783.
[46] H. Topsøe, B.S. Clausen, N.-Y. Topsøe, E. Pedersen, W. Niemann, A. Müller, H. Bögge, B. Lengeler, J. Chem. Soc. Faraday Trans. 1 83 (1987) 2157 (Faraday Symposium 21).
[47] N.-Y. Topsøe, H. Topsøe, Bull. Soc. Chim. Belg. 90 (1981) 1311.
[48] E.G. Derouane, E. Pedersen, B.S. Clausen, Z. Gabelica, H. Topsøe, J. Catal. 107 (1987) 587.
[49] T. Zeng, X.-D. Wen, G.-S. Wu, Y.-W. Li, H. Jiao, J. Phys. Chem. B 109 (2005) 2846.
[50] T. Zeng, X.-D. Wen, Y.-W. Li, H. Jiao, J. Mol. Catal. A: Chem. 241 (2005) 219.
[51] T. Zeng, X.-D. Wen, Y.-W. Li, H. Jiao, J. Phys. Chem. B 109 (2005) 13704.
[52] M.A. Lélias, A. Travert, J. van Gestel, F. Maugé, J. Phys. Chem. B 110 (2006) 14001.
[53] X.-D. Wen, T. Zeng, H. Jiao, J. Phys. Chem. B 110 (2006) 14004.
[54] X.-D. Wen, Y.-W. Li, J. Wang, H. Jiao, J. Phys. Chem. B 110 (2006) 21060.
[55] X.-D. Wen, J. Ren, Y.-W. Li, J. Wang, H. Jiao, Chem. Phys. Lett. 436 (2007) 209.
[56] S. Helveg, J.V. Lauritsen, E. Lægsgaard, I. Stensgaard, J.K. Nørskov, B.S. Clausen, H. Topsøe, F. Besenbacher, Phys. Rev. Lett. 84 (2000) 951.
[57] M.V. Bollinger, J.V. Lauritsen, K.W. Jacobsen, J.K. Nørskov, S. Helveg, F. Besenbacher, Phys. Rev. Lett. 87 (2001) 196803.
[58] J.V. Lauritsen, S. Helveg, E. Lægsgaard, I. Stensgaard, B.S. Clausen, H. Topsøe, F. Besenbacher, J. Catal. 197 (2001) 1.
[59] J.V. Lauritsen, M. Nyberg, R.T. Vang, M.V. Bollinger, B.S. Clausen, H. Topsøe, K.W. Jacobsen, E. Lægsgaard, J.K. Nørskov, F. Besenbacher, Nanotechnology 14 (2003) 385.
[60] J.V. Lauritsen, M.V. Bollinger, E. Lægsgaard, K.W. Jacobsen, J.K. Nørskov, B.S. Clausen, H. Topsøe, F. Besenbacher, J. Catal. 221 (2004) 510.
[61] V. Lauritsen, M. Nyberg, J.K. Nørskov, B.S. Clausen, H. Topsøe, E. Lægsgaard, F. Besenbacher, J. Catal. 224 (2004) 94.
[62] J.V. Lauritsen, J. Kibsgaard, G.H. Olesen, P.G. Moses, B. Hinnemann, S. Helveg, J.K. Nørskov, B.S. Clausen, H. Topsøe, E. Lægsgaard, F. Besenbacher, J. Catal. 249 (2007) 218.
[63] J.V. Lauritsen, F. Besenbacher, Adv. Catal. 50 (2006) 97.
[64] L.S. Byskov, B. Hammer, J.K. Nørskov, B.S. Clausen, H. Topsøe, Catal. Lett. 47 (1997) 109.
[65] L.S. Byskov, J.K. Nørskov, B.S. Clausen, H. Topsøe, J. Catal. 187 (1999) 109.
[66] M.V. Bollinger, K.W. Jacobsen, J.K. Nørskov, Phys. Rev. B 67 (2003) 854101.
[67] P. Raybaud, J. Hafner, G. Kresse, S. Kasztelan, H. Toulhoat, J. Catal. 189 (2000) 129.
[68] P. Raybaud, J. Hafner, G. Kresse, S. Kasztelan, H. Touloat, J. Catal. 190 (2000) 128.
[69] S. Cristol, J.-F. Paul, E. Payen, D. Bougeard, S. Clémendot, F. Hutschka, J. Phys. Chem. B 104 (2000) 11220.
[70] V. Alexiev, R. Prins, Th. Weber, Phys. Chem. Chem. Phys. 3 (2001) 5326.
[71] H. Schweiger, P. Raybaud, G. Kresse, H. Toulhoat, J. Catal. 207 (2002) 76.
[72] B. Hinnemann, J.K. Nørskov, H. Topsøe, J. Phys. Chem. B 109 (2005) 2245.
[73] M. Sun, J. Adjaye, A.E. Nelson, Appl. Catal. A: Gen. 263 (2004) 131.
[74] B. Hinnemann, P.G. Moses, J. Bonde, K.P. Jørgensen, J.H. Nielsen, S. Horch, I. Chorkendorff, J.K. Nørskov, J. Am. Chem. Soc. 127 (2005) 5308.
[75] M. Sun, A.E. Nelson, J. Adjaye, Catal. Today 105 (2005) 36.
[76] P. Raybaud, Appl. Catal. A 322 (2007) 76.
[77] P.G. Moses, B. Hinnemann, H. Topsøe, J.K. Nørskov, J. Catal. 248 (2007) 188.
[78] P.G. Moses, B. Hinnemann, H. Topsøe, J.K. Nørskov, J. Catal. 268 (2009) 201.
[79] F. Besenbacher, M. Brorson, B.S. Clausen, S. Helveg, B. Hinnemann, J. Kibsgaard, J.V. Lauritsen, P.G. Moses, J.K. Nørskov, H. Topsøe, Catal. Today 130 (2008) 86.
[80] B. Temel, A.K. Tuxen, J. Kibsgaard, N.-Y. Topsøe, B. Hinnemann, K.G. Knudsen, H. Topsøe, J.V. Lauritsen, F. Besenbacher, J. Catal. 271 (2010) 280.
[81] N.-Y. Topsøe, H. Topsøe, F.E. Massoth, J. Catal. 119 (1989) 252.
[82] Á. Logadóttir, P.G. Moses, B. Hinnemann, N.-Y. Topsøe, K.G. Knudsen, H. Topsøe, J.K. Nørskov, Catal. Today 111 (2006) 44.
[83] E. Lægsgaard, F. Besenbacher, K. Mortensen, I. Stensgaard, J. Microsc. 152 (1988) 3.
[84] J. Kibsgaard, J.V. Lauritsen, E. Lægsgaard, B.S. Clausen, H. Topsøe, F. Besenbacher, J. Am. Chem. Soc. 128 (2006) 13950.
[85] A. Tuxen, J. Kibsgaard, H. Gøbel, E. Lægsgaard, H.Topsøe, J.V. Lauritsen, F. Besenbacher, ACS Nano 4 (2010) 4677.
[86] B. Hammer, L.B. Hansen, J.K. Nørskov, Phys. Rev. B 59 (1999) 7413.
[87] S.R. Bahn, K.W. Jacobsen, Comput. Sci. Eng. 4 (2002) 56.
[88] H.J. Monkhorst, J.D. Pack, Phys. Rev. B 13 (1976) 5188.
[89] K. Laasonen, A. Pasquarello, R. Car, C. Lee, D. Vanderbilt, Phys. Rev. B 47 (1993) 10142.
[90] D. Vanderbilt, Phys. Rev. B 41 (1990) 7892.

[91] N. Troullier, J.L. Martins, Phys. Rev. B 43 (1991) 1993.
[92] J.V. Lauritsen, J. Kibsgaard, G.H. Olesen, P.G. Moses, B. Hinnemann, S. Helveg, J.K. Nørskov, B.S. Clausen, H. Topsøe, F. Besenbacher, J. Catal. 249 (2007) 220.
[93] J.P. Perdew, J.A. Chevary, S.H.Vosko.K.A. Jackson, M.R. Pederson, D.J. Singh, C. Fiolhais, Phys. Rev. B 46 (1992) 6671.
[94] Th. Böker, R. Severin, A. Müller, C. Janowitz, R. Manzke, D. Voss, P. Krüger, A. Mazur, J. Pollman, Phys. Rev. B 64 (2001) 235305.
[95] K. Nakamoto, Infrared Spectra of Inorganic and Coordination Compounds, John Wiley & Sons, New York, 1970.

[96] Y. Okamoto, A. Maezawa, T. Imanaka, J. Catal. 120 (1989) 29.
[97] N.-Y. Topsøe, H. Topsøe, J. Catal. 139 (1993) 641.
[98] R. Candia, J. Villadsen, N.-Y. Topsøe, B.S. Clausen, H. Topsøe, Bull. Soc. Chim. Belg. 93 (1984) 763.
[99] Y.V. Joshi, P. Ghosh, M. Daage, W.N. Delgass, J. Catal. 257 (2008) 71.
[100] C. Arrouvel, M. Digne, M. Breysse, H. Toulhoat, P. Raybaud, J. Catal. 222 (2004) 152.
[101] C. Arrouvel, M. Breysse, H. Toulhoat, P. Raybaud, J. Catal. 232 (2005) 161.
[102] D. Costa, C. Arrouvel, M. Breysse, H. Touloat, P. Raybaud, J. Catal. 246 (2007) 325.